Artigo

PREPARATION AND PERFORMANCE OF MAGNETIC ZIRCONIUM-IRON OXIDE NANOPARTICLES LOADED ON PALYGORSKITE IN THE ADSORPTION OF PHOSPHATE FROM WATER

Xiaoshuang Song[a], [iD], Yanling Hao[a],*, Qiqi Gao[a] and Long Cheng[a]

[a]School of Chemical and Biological Engineering, Lanzhou Jiaotong University, Lanzhou, China

Magnetic zirconium-iron oxide nanoparticles loaded on palygorskite as a low-cost adsorbent was produced by one-step co-precipitation technique and its properties for phosphate adsorption were overall investigated. The Brunauer Emmett Teller (BET) specific surface area analysis, scanning electron microscopy (SEM), thermo gravimetric analysis (TGA), Fourier transform infrared spectroscopy (FTIR), X-ray diffraction (XRD) and X-ray photoelectron spectroscopy (XPS) were used to characterize the adsorbent and evaluate the adsorption interactions. The influences of pH, ionic strength and coexisting ions on phosphate adsorption were measured with a discussion of the adsorption mechanism. Results indicated that no very noticeable changes on the surface properties, structure and phosphate adsorption capacity be found for the magnetic zirconium-iron oxide nanoparticles loaded on palygorskite or not. The adsorption kinetics fitted to the pseudo-second-order model and adsorption isotherm followed Langmuir equation and Dubinin-Radushkevich equation. The phosphate adsorption was slightly affected by ionic strength and highly dependent on pH, *i.e.* increasing pH sharply restrained adsorption under neutral and alkaline conditions. The surface OH groups in the adsorbent processed an important role in adsorption and the adsorption mechanism conformed to ion exchange and complex. The adsorbent could be conveniently regenerated and effectively reused.

Keywords: magnetic; zirconia; palygorskite; phosphate; adsorption.

INTRODUCTION

Phosphorus, as one of essential nutrient element, makes significant contribution to energy transport and supports the growth of biological organisms. It is also an important material for agricultural and industrial products. Nevertheless, the discharge of extensive phosphate containing wastewater into the aquatic environment resulting from anthropogenic activities leads to the eutrophication of receiving waters, which causes the over growth of algae, depletion of dissolved oxygen, deterioration of water quality, and depopulation of aquatic animals.[1,2] It is of significant importance to control the amounts of phosphorous in water to maintain aquatic ecosystem health and a green environment for the forthcoming generation.[3]

Many kinds of treatment techniques, such as adsorption, chemical precipitation, ion exchange, biological process, membrane, reverse osmosis, have been developed to eliminate phosphate pollution prior to wastewater discharge. Among these approaches, adsorption is generally considered to be a common method ideal for phosphate removal in water.[4,5] Comparatively, the adsorption has some advantages, such as easy for operation, low-cost, high efficiency, environmentally friendly and fast adsorption rate. It also could be easily applied for phosphate removal at a wide range of phosphate concentration.[6,7] The sorption efficiency is more dependent on the nature of adsorbent and therefore, in recent years considerable attention has been paid to the investigation of different types of low-cost and non-toxic sorbents based on economic and environmental concerns. Different clay-based adsorbents have been investigated recently, such as natural clinoptilolite,[8] montmorillonite,[9,10] bentonite,[11,12] metal-modified diatomite[13,14] and zeolite[15,16] among others. Palygorskite is a crystalline hydrated magnesium aluminium silicate mineral with unique three dimensional structures and has a fibrous morphology, and it is abundant, inexpensive, available,

chemically, mechanically, and environmentally stable.[17] Its high surface area, sorption ability and ion exchange properties enable it to be drawn upon for developing adsorbent as matrix material to enhance contaminant control.[18]

Zirconium oxides (zirconium oxides or hydrous zirconium oxides) have a strong affinity to phosphate and desorption for recycling. They are non-toxic and highly resistant to attack by acids/bases, oxidizing and reducing agents, and also they have and very low solubility in water as well as remarkable selectivity in adsorbing phosphate in the presence of other anions.[19,20] In order to improve the adsorption capacity and recyclability and avoid the drawback of separation inconvenience, it is of particular significance to develop low-cost adsorbent with zirconium loaded on some support material.[21,22]

In the present essay, the palygorskite clay supported zirconium oxide incorporating magnetic iron to facilitate phosphate adsorption as well as magnetic separation and recover of adsorbent. The magnetic zirconium-iron oxide nanoparticles loaded on palygorskite were prepared via one-step co-precipitation techniques and characterized by SEM, FTIR, TG and XRD. Their phosphate removal performance was investigated by batch experiments with a discussion of adsorption mechanism. The current study is expected to be helpful for the application of the loaded magnetic adsorbent to remove phosphate from water and control eutrophication of water bodies.

EXPERIMENTAL

Materials and reagents

Palygorskite clay with the average diameter of 200 meshes was provided by XingGuang Technology Co., Ltd., Gansu, China. All chemicals were of analytical grade and directly used without further purification. Zirconium oxychloride octahydrate (ZrOCl₂·8H₂O) received from Sinopharm Chemical Reagent Co., Ltd. Shanghai, China, Ferric chloride (FeCl₃·6H₂O), ferrous sulfate (FeSO₄·7H₂O) and sodium hydroxide (NaOH) purchased from Tianjin Chemical Co.,

*Corresponding author. E-mail addresses: 137701321@qq.com (Yanling Hao), 1435381545@qq.com (Xiaoshuang Song)

China were all used in the preparation of adsorbents with incorporation of palygorskite. Potassium dihydrogen phosphate (KH_2PO_4), ammonium heptamolybdate ((NH_4)$_6Mo_7O_{24}.H_2O$) and ascorbic acid from Sinopharm Chemical Reagent Co., Ltd. China were used for phosphate standard solution and determination. The stock solution of phosphate was prepared by dissolving an accurately weighted of anhydrous KH_2PO_4 in distilled water and the standard phosphate solutions were prepared by dilution of the stock solution with doubly distilled water.

Preparation of adsorbent

Magnetic zirconium-iron oxide nanoparticles were synthesized by a co-precipitation method. A series of mixture solution containing $FeSO_4 \cdot 7H_2O$ (0.25 mol L^{-1}), $FeCl_3 \cdot 7H_2O$ (0.50 mol L^{-1}) and different amount of $ZrOCl_2 \cdot 8H_2O$ were prepared by dissolving corresponding solute in 250 mL distilled water. An amount of 0.4 mol L^{-1} NaOH solution was injected drop-wisely into the above solution with vigorous agitation at room temperature until the pH of the solution reached 8~8.5. The resulting mixture were aged at 60 °C in a constant temperature water bath for 18 h and then the precipitates were collected and washed with distilled water and ethanol to be recovered twice. Finally, the product is oven-dried at 60 °C for 24 hours, ground to pass through 100 mesh sieves and kept at desiccator for further use. The adsorbent sample without zirconium was noted MF and the samples with zirconium and iron molar ratios of 1/4, 1/2 and 1/1 were named MZF1, MZF2, MZF3, respectively.

Palygorskite clay was purified by the reported process.[23] 1.0, 1.5 and 2.0 g palygorskite (PAL) were dispersed into 100 mL distilled water by ultrasonic dispersion for 10 min to obtain a stable suspension, respectively. The mixture solution containing $FeSO_4 \cdot 7H_2O$ (0.25 mol L^{-1}), $FeCl_3 \cdot 7H_2O$ (0.50 mol L^{-1}) and of $ZrOCl_2 \cdot 8H_2O$ (0.375 mol L^{-1}) was added into the suspension of PAL under intensive stirring and the mixture was stirred at 60 °C for 2 h followed by withdrawing under room temperature. Subsequently, the pH of the mixed suspensions were adjusted to a range of 8.5~9.0 via addition dropwise an amount of 0.4 mol L^{-1} NaOH solution into the suspensions and resulting suspensions were aged at 60 °C for 18 h. The sediments were separated, rinsed and dried and the magnetic zirconium-iron oxide nanoparticles loaded on PAL were obtained. The products were named MZF/P1, MZF/P2 and MZF/P3, respectively.

Material characterization

The FTIR spectroscopy of adsorbent samples before and after phosphate adsorption were measured on FTIR spectrometer (VERTEX 70, Bruker Scientific Instruments Co., Germany) with KBr powder as background material and in the range of 400 to 4000 cm^{-1} at a resolution of 4 cm^{-1}. The XRD patterns of the samples were collected on a Bruker SMART APEX II powder diffraction meter (Bruker Scientific Instruments Co., Germany) using a Cu-Kα radiation. The surface morphologies of samples were observed by a SEM (Hitachi SU8020, Hitachi High-Tech Co., Ltd., Japan) operating at a voltage acceleration of 15 kV. The BET specific surface areas of the samples were analyzed by nitrogen adsorption-desorption measurement through an ASAP 2010 instrument (Micromeritics Instrument Co., Norcross, GA, USA). The surface charge properties were characterized by zeta potential (Nano ZS90, Malvern Instruments, UK). The thermal analysis data were collected using STA449F3 thermo analyzer (Netzsch Co., Germany), heating from 40 to 800 °C under a nitrogen atmosphere. The valence of specific elements before and after adsorption was analyzed by XPS spectra (PHI 5702 spectrometer, Physics Electronics Inc., USA). The results were corrected by C1s at a binding energy of 284.6 eV.

Adsorption experiments

To evaluate the adsorption performance of the adsorbents, the batch adsorption experiments were carried out at the different initial concentration of phosphate for different uptake time. A series of 100 mL conical beaker containing 50 mg of adsorbent and 20 mL of phosphate solution were placed on a constant temperature bath oscillator to vibrate with a speed of 150 rpm at 25 °C. Then the adsorbents were separated from the solution and the residual concentration of phosphate was determined by the molybdenum-blue ascorbic method with a detecting wavelength of 700 nm.[24] All the experiments were performed in triplicate and the data were expressed as the mean.

The influence of contact time on phosphate adsorption capacity was researched in different time intervals ranging from 2 min to 360 min with initial phosphate concentration of 50 mg/L and 100 mg/L at pH 4.5 of the initial phosphate solution. The adsorption capacity was calculated according to Eq (1):

$$Q_t = \frac{(c_0 - c_t)V}{m} \tag{1}$$

Adsorption isotherm was investigated by determining adsorption capacity at 25 °C temperature and different initial concentrations of phosphate from 10 to 200 mg/L at fixed pH 4.5 under 300 min of the contact time to obtain adsorption equilibrium. Phosphate adsorption capacity was calculated according to Eq (2):

$$Q_e = \frac{(c_0 - c_e)V}{m} \tag{2}$$

where Q_t and Q_e are the adsorption capacity at time t and equilibrium (mg g^{-1}), respectively, c_0, c_t, and c_e are the solution concentration of phosphate at the initial time, time t and equilibrium (mg L^{-1}), respectively. V is the volume of the phosphate solution (L) and m is the mass of adsorbent used (g).

The effects of pH and ionic strength on phosphate adsorption were studied over the pH range of 2-12 in the presence of NaCl solution with 0, 0.01, 0.1 and 0.5 mol L^{-1} of concentrations at 25 °C. The initial concentration of phosphate solution was 50 mg L^{-1} and the uptake time was 300 min. The initial pH of the phosphate solution was adjusted by the addition of 0.1 mol L^{-1} solution of HCl or NaOH. The effects of coexisting anions on phosphate adsorption at 25 °C were also examined. The initial concentration of phosphate was fixed at 50 mg L^{-1} and the uptake time was 300 min.

Desorption, regeneration and recyclability experiments

Desorption experiments were conducted using 1.0 mol L^{-1} NaOH aqueous solution as desorption solution for estimating the regeneration of the adsorbent. The initial phosphate concentration was 50 mg L^{-1} and the process was operated at 25 °C. The adsorbent previously saturated with phosphate was separated from the solution and then mixed with 100 mL NaOH solution under stirring for 24 h. Subsequently, the adsorbent was separated and washed thoroughly with distilled water for three times. Eventually, the regenerated adsorbent after drying was used again for phosphate adsorption. The adsorption-desorption cycles were performed for five times. Experiments were undertaken in triplicate and the mean data were reported.

RESULTS AND DISCUSSION

Selection of adsorbents

Comparison of adsorption over samples

The adsorption capacities of adsorbents are shown in Figure 1. It was obvious that all magnetic zirconium-iron oxide nanoparticles possessed much higher adsorption capacity than MF and the rise of Zr/Fe molar ratio in MZF led to an increase in adsorption capacity, accompanying significant increase for MZF3 and MZF2 than that for MZF1, but a slightly large for MZF3 than that for MZF2. This could be explained that the surface of magnetic zirconium-iron oxide became rougher with the increase of Zr/Fe molar ratio.[25] Loading of magnetic zirconium-iron oxide nanoparticles on PAL should cause a decrease in phosphate adsorption capacity due to PAL could hardly be used as active adsorbent for phosphate. Comparing the reduction in adsorption capacity, the MZF/P3 had a more obvious degree than MZF/P2 and MZF/P1. Considering the consumption of product costs, the MZF2 and MZF/P2 displayed insignificant disadvantage than their counterparts, thus they was selected as the adsorbents for further studies and were hereinafter briefly noted MZF and MZF/P, respectively.
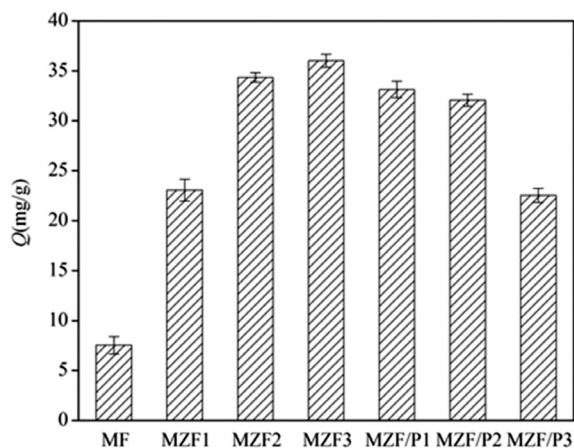

Figure 1. *Adsorption capacity of samples (initial phosphate concerntration: 10 mg L^-1; adsorbent dose: 0.25 g L^-1; contact time: 300 min; temperature: 25 °C; pH:4.5~4.7)*

BET surface area, SEM and thermal stability

The structure properties of PAL and the adsorbents studied are summarized in Table 1. According to the data the MZF samples had larger BET surface area than Zr-Fe binary oxides previously reported.[26] It can be seen that the MF had a very low surface area and a smaller pore volume following a larger pore size. With an increase of Zr/Fe molar ratio in MZF the specific surface areas of MZF enhanced, the pore volumes slightly enlarged and pore sizes had tiny reduce. For the MF, the higher magnetization is not conducive to the dispersion of iron oxide and the crystalline structure and large particle size lead to its low surface area and pore volume. The increase of Zr content in MZF caused lower magnetization which had the effect to disperse iron oxides and zirconium oxides more uniformly.[25] The hydrous zirconia had amorphous structure and it occupied the surface of the composite while the magnetite was mainly located inside the aggregates.[27] Therefore significant enhancement of specific surface area as well as larger pore volume and smaller pore size appeared in MZF.

The specific surface area and pore volume of MZF/P were significantly higher than PLA and lower than MZF2. The increase in the amount of PAL leads to a decrease in the specific surface area and pore volume, but the pore size was approximately equal to MZF2 and PLA. It might be interpreted that the deposition of magnetic zirconium-iron oxide on PAL did not result in the collapse of the pore structure of PAL. Generally, adsorbent with a smaller pore size and larger pore volume possesses a superior surface area.[25]

The morphological characteristics of the MZF and MZF/P were studied and their SEM images were displayed in Figure 2. It could be seen that the surface of particles for MZF was rough, uneven and loose with lots of protuberances led to a porous structure. The magnetic zirconium-iron oxide nanoparticles precipitated on the palygorskite basically maintained its rough and uneven surface, while the degree of fluffy was reduced. It was consistent with the decrease of the specific surface area and pore volume for the MZF/P.

The physical stability of the prepared MZF/P was studied by TGA analysis which is shown in Figure 3. The TGA curve of MZF/P was taken under nitrogen atmosphere there was three weight loss steps. The first step of weightlessness between 0 and 100 °C indicated a loss of 5.53% of water molecules in MZF/P. The second of weight losses started between 100 °C and 600 °C which indicated the thermal decomposition of magnetic zirconium-iron oxide and palygorskite released a loss of 7.65% of the volatile materials. The final weight
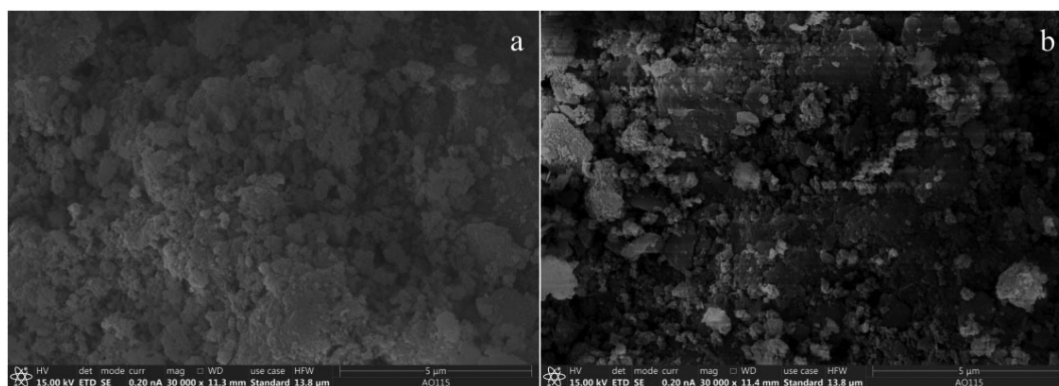
Table 1. Structure and pore properties of the samples

Samples	PAL	MF	MZF1	MZF2	MZF3	MZF/P1	MZF/P2	MZF/P3
S_{BET} (m² g⁻¹)	58.39	56.27	105.07	129.75	135.20	118.25	109.09	98.36
V_t (cm³ g⁻¹)	0.102	0.205	0.211	0.219	0.223	0.217	0.214	0.203
d_P (nm)	6.39	12.06	7.55	7.02	4.73	6.68	6.71	6.89

Figure 2. *SEM image of (a) MZF and (b) MZF/P*

loss was observed at 600-800 °C and there was no significant change for 86.82% of initial mass. Thus MZF/P is provided with practical thermal stability.
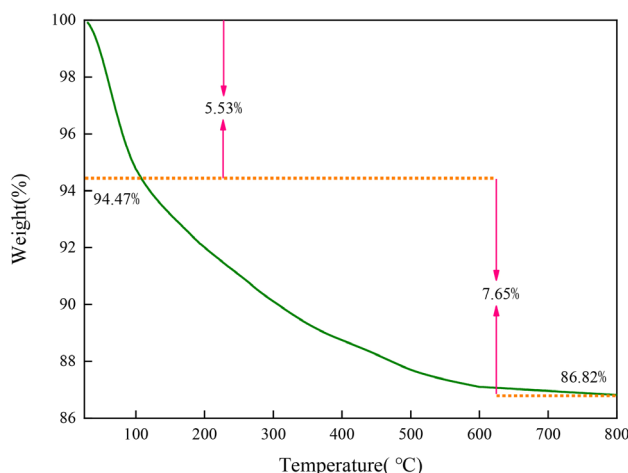

Figure 3. *TGA of MZF/P under nitrogen atmosphere*

Adsorption kinetics

Adsorption kinetics is an important parameter for evaluating the efficiency of adsorption processes and its related studies was conducted to understand the adsorption mechanism. The effect of contact time on the adsorption was investigated for an initial concentration of 50 mg L^{-1} and 100 mg L^{-1} and a fixed pH solution of 4.5~4.7. It was observed in Figure. 4(a) that the adsorption process took place in two steps: a rapid uptake of the beginning and a slower adsorbing stage until equilibrium state was reached. Within original 90 min about 90% of the phosphate adsorption was achieved and the

adsorption gradually slows down and becomes stable from 180 min to 300 min. Therefore, 300 min was selected as the equilibrium time for the research of adsorption isotherm.

Generally, the physicochemical characteristics of adsorbent and the diffusion process occurring in adsorption system can be speculated by adsorption kinetics analysis. The pseudo-first-order, pseudo-second-order, and intra-particle diffusion models were applied to fit experimental data.

The mathematical forms of pseudo-first-order and pseudo-second-order kinetic models are expressed as Eqs. (3) and (4), respectively.

$$\log(Q_e - Q_t) = \log Q_e - k_1 t / 2.303 \tag{3}$$

$$\frac{t}{Q_t} = \frac{1}{k_2 Q_e^2} + \frac{t}{Q_e} \tag{4}$$

where Q_e is the equilibrium adsorption capacity (mg g^{-1}); Q_t is the adsorption capacity (mg g^{-1}) at time t (min); k_1 and k_2 are pseudo-first-order and pseudo-second-order rate constants, respectively.

The fitting curves and kinetic parameters obtained from the regression of the above two equations are shown in Figure 4(b), (c) and Table 2. Obviously, the values of R^2 of pseudo-second-order equation were all greater than that of pseudo-first-order equation and closer to 1. Moreover, the experimental values of equilibrium adsorption capacity Q_e were more consistent with the calculated values from pseudo-second-order equation. It suggested that the dynamic feature of phosphate adsorbed at initial phosphate concentration of 50 and 100 mg L^{-1} all could be satisfactorily depicted by the pseudo-second-order model, which implied that chemisorption dominated the adsorption process implicating exchange of electrons or valence forces through sharing among sorbate and sorbent. Similar findings about the phosphate adsorption on other adsorbents were reported by Wang *et al.*[28] and Xiong *et al.*[29] Based on pseudo-second-order
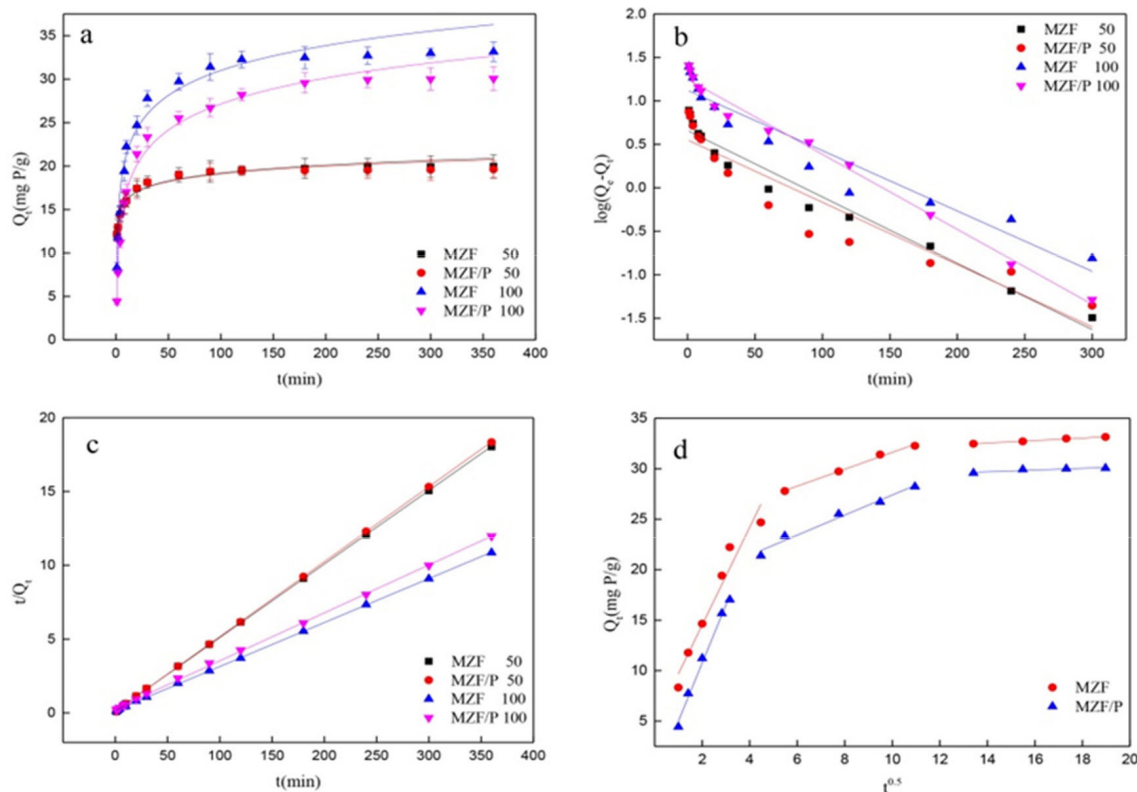

Figure 4. (*a*) *The influence of contact time on the absorption by MZF and MZF/P;* (*b*) *fitting with pseudo-first-order model;* (*c*) *pseudo-second-order model;* (*d*) *intra-particle diffusion model. (initial phosphate concerntration: 50 mg/L or 100 mg/L; adsorbent dose: 2.5 g/L; pH:4.5~4.7; temperature: 25 °C)*

Table 2. Kinetic parameters of adsorption based on the pseudo-first-orde and pseudo-second-order model

c_0 (mg/L)	Adsorbents	$Q_{e,exp}$ (mg/g)	pseudo-first-order			pseudo-second-order		
			$k_1 \times 10^3$ (min^{-1})	$Q_{e,cal}$ (mg g^{-1})	R^2	$k_2 \times 10^3$ (g mg^{-1} min^{-1})	$Q_{e,cal}$ (mg g^{-1})	R^2
50	MZF	19.958	16.58	4.550	0.9634	21.32	20.040	0.9999
50	MZF/P	19.622	17.50	3.435	0.8633	28.23	19.685	1.0000
100	MZF	33.144	15.98	13.241	0.9178	5.41	34.165	0.9999
100	MZF/P	30.062	19.87	17.726	0.9866	3.79	30.778	0.9996

model, the rate constant k_2 presented smaller values at higher initial phosphate concentration. No significant difference occurred on the values of k_2 and Q_e for adsorbent MZF/P and MZF.

The intra-particle diffusion model was employed to estimate the adsorption pathways and the rate-determining steps.[30] It was usually described by the following Eq. (5):

$$Q_t = k_p t^{0.5} + C \qquad (5)$$

where Q_t is adsorption capacity (mg g^{-1}) at time t (min); k_p is the intra-particle diffusion rate constant (mg g^{-1} min$^{-0.5}$) and C is related to the thickness of the boundary layer.

Figure 4(d) displayed that the plots of Q_t versus t$^{0.5}$ for phosphate adsorption on MZF and MZF/P at initial phosphate concentration of 100 mg L^{-1} and their multi-linearity correlation indicated that the adsorption process involved more steps.[2] Firstly, the adsorption underwent a very fast stage within the initial 20 min during which the phosphate maybe quickly transported from aqueous phase to the surface of adsorbent under the concentration gradient force. Secondly, as the exterior surface of adsorbents was saturated, phosphate entered into the pore of adsorbents and was adsorbed by its interior surface. During this period of 20 to 150 min the intra-particle diffusion determined the adsorption rate. Finally, the adsorption process reached the equilibrium stage with the saturation of the adsorbent surface and the termination of the intra-particle diffusion after 180 min.

The rate constant k_p and C were fitted from the intra-particle diffusion model were listed in Table 3. It was seen that the rate constants were in the order of $k_{p,1} > k_{p,2} > k_{p,3}$ for the two sorbents. The values of C being proportional to the thickness of the boundary layer were larger than 0 postulating that the intra-particle diffusion was not uniquely control the rate.[2] The MZF/P presented almost similar characteristic and rate constant with MZF.

Adsorption isotherms

The phosphate adsorption isotherms of MZF and MZF/P at 25 °C were summarized in Figure 5 (a) and these demonstrated enhanced adsorption capacity with the increase of initial concentrations of phosphate solutions and gradually reached saturation. The Freundlich and Langmuir isotherm equations were employed to describe the adsorption isotherms and their hypothetic parameters were estimated to understand the surface properties and adsorption mechanism.

Freundlich equation based on the adsorption on a heterogeneous surface, and it is given by:

$$\ln Q_e = n \ln c_e + \ln k_F \qquad (6)$$

Langmuir isotherm which based on the assumption of a homogeneous surface of the solid adsorbent and the monolayer adsorption is represented as:

$$\frac{c_e}{Q_e} = \frac{c_e}{Q_m} + \frac{1}{Q_m K_L} \qquad (7)$$

where c_e is the equilibrium concentration of the phosphate (mg L^{-1}); Q_e is the equilibrium adsorption capacity (mg g^{-1}); Q_m is the adsorption capacity when the surface is covered by a monolayer of adsorbate (mg g^{-1}); K_L is the Langmuir constant (L g^{-1}); K_F related to the adsorption capacity and n stood for the adsorption intensity.

The adsorption isotherms can also be analyzed by the Dubinin-Radushkevich (D-R) equation, which can be estimated not only the maximum adsorption capacity, but also a value of mean energy of sorption to the system. In deriving this equation, the amount adsorbed corresponding to adsorbate concentration is assumed to be a function of the Polanyi potential, ε.[31]

$$\ln Q_e = \ln Q_{DR} - \beta \varepsilon^2 \qquad (8)$$

$$\varepsilon = RT \ln\left(1 + \frac{1}{c_e}\right) \qquad (9)$$

$$E_s = \frac{1}{\sqrt{2\beta}} \qquad (10)$$

where Q_{DR} is the maximum adsorption capacity that the phosphate can be adsorbed (mg g^{-1}); R the universal gas constant (8.314 J mol^{-1} K^{-1}); T the absolute temperature (K); β (mol^2 kJ^{-2}) is a constant giving the mean energy of sorption E_s (kJ mol^{-1}) of adsorption per molar of the adsorbate when it is transferred to the surface of the solid from infinity in the solution.

The parameters by fitting the isotherms data to the Langmuir, the Freundlich, and the D-R equation were listed in Table 4. As be seen, it manifested from the values of R^2 that the adsorption isotherms data were slightly better suitable for the Langmuir equation than the Freundlich equation. The results indicated that the adsorption process likely involved the chemical mechanism and the adsorption conducted in a monolayer fashion. The maximum adsorption capacity Q_m and the Langmuir constant K_L of phosphate on the MZF/P were 38.168 mg g^{-1} and 0.241 L mg^{-1}, respectively, which were both slightly lower than those of the MZF. This was consistent with the specific surface area of the adsorbents and the dominant contribution of the zirconium to

Table 3. Kinetic parameters of adsorption based on the intra-particle diffusion model

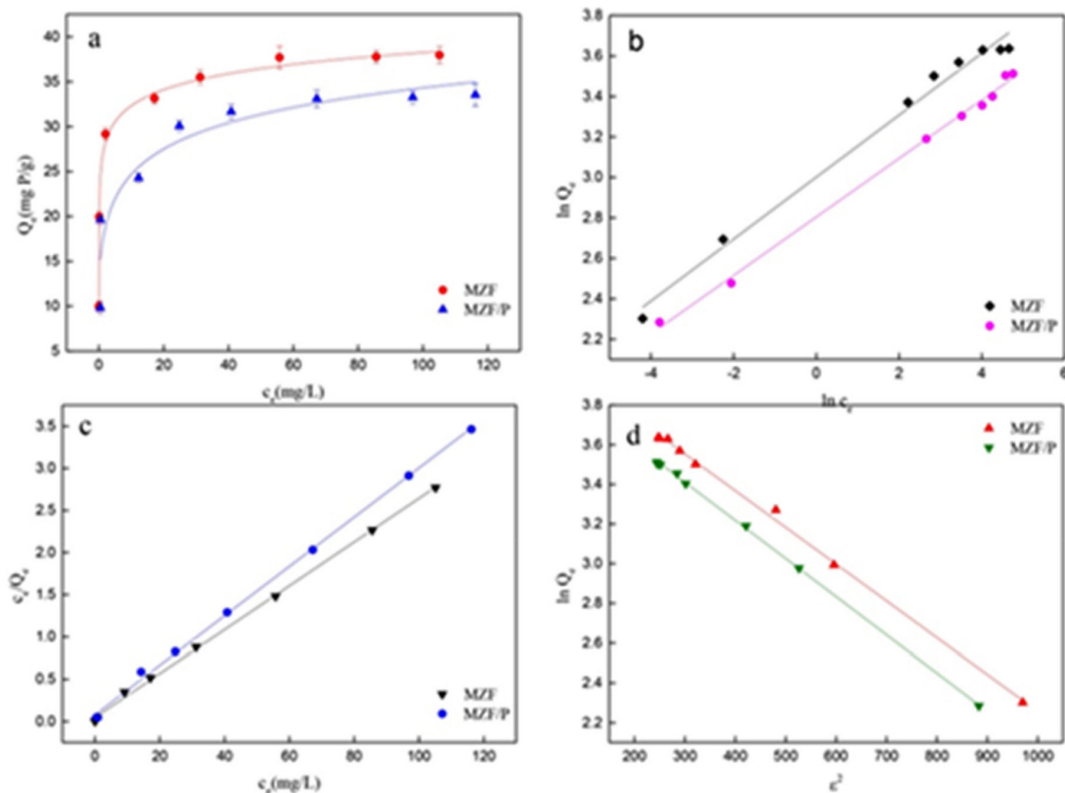| Adsorbents	$k_{p,1}$ (mg g^{-1} min$^{-0.5}$)	C (mg/g)	R^2	$k_{p,2}$ (mg g^{-1} min$^{-0.5}$)	C (mg g^{-1})	R^2	$k_{p,3}$ (mg g^{-1} min$^{-0.5}$)	C (mg g^{-1})	R^2
MZF	4.840	4.843	0.9364	0.837	23.258	0.9913	0.124	30.809	0.9902
MZF/P	5.756	0.765	0.9897	0.994	17.459	0.9714	0.085	28.504	0.9618

Figure 5. *(a) Adsorption isotherms; (b) linear Freundlich adsorption isotherms; (c) linear Langmuir adsorption isotherms; (d) linear D-R adsorption isotherms (contact time: 300 min; adsorbent dose: 2.5 g/L; pH:4.5~4.7; temperature: 25 °C)*

Table 4. Regression parameters of adsorption isotherms

	Freundlich equation			Langmuir equation			D-R equation			
	K_F	n	R^2	Q_m (mg g^{-1})	K_L (L mg^{-1})	R^2	Q_m (mg g^{-1})	$\beta \times 1000$ (mol^2 kJ^{-2})	E_s (kJ mol^{-1})	R^2
MZF	15.532	0.2409	0.9809	43.373	0.332	0.9918	59.973	1.847	16.453	0.9875
MZF/P	13.342	0.2395	0.9818	38.168	0.241	0.9842	53.715	1.924	16.121	0.9948

phosphate adsorption.[32] A larger value of the K_L implies a stronger adsorption, *i.e.* a higher average energy on the adsorptive sites. Therefore the average energy of the adsorptive sites of MZF/P was insignificantly lower than that of MZF. The D-R equation could also well describe the adsorption isotherms. The values of β were less than unity and so implied that the adsorbents had fine micropores and the surface heterogeneity might be arisen from the pore structure as well as adsorbate-adsorbent interactions.[33] The mean energies of sorption estimated from the D-R equation, without significant difference, were 16.45 and 16.12 kJ mol^{-1} for phosphate adsorption on MZF and MZF/P, respectively, These values approximately lied within 8-16 kJ mol^{-1} of the typical range of mean energy of sorption envisaged for the ion-exchange mechanism,[34] it was expected that phosphate removed from aqueous solutions through an ion exchange interaction.

The results of maximum phosphate adsorption capacity Q_m compared with adsorbents reported in the other studies are listed in Table 5.

Table 5. Phosphate adsorption capacity of adsorbents reported in the literature

Adsorbent	Maximum adsorption(mg/g)
This study	38.168
zirconium (IV) hydroxide[19]	30.4
MZION[20]	21.3
Zr-A[22]	24.55
ZrO$_2$[36]	29.71

Influence of pH, ionic strength and coexisting anions

The adsorption capacities of phosphate on MZF/P at an initial concentration of 50 mg L^{-1} under different conditions of pH and ionic strength were shown in Figure 6(a). The phosphate uptake was considerably controlled by the pH and the increase of pH led to continuous decrease of phosphate adsorption over the examined pH range of 2-12. The adsorption capacities were higher and displayed little difference under the acidic condition with pH lower than about 5.0, whereas a sudden reduce happened within pH range of 5-12. The ionic strength had a certain influence on the phosphate adsorption and the effect was more evident in the high pH range than that in low pH.

The pH dependency should be related to both the surface properties of the adsorbent and to the nature of phosphate.[35] The surface zeta potentials of the MZF/P versus pH was presented in Figure 6(b). The increase of pH led to more negative surface potential of MZF/P and its isoelectric point (pH$_{pzc}$) was found to be about 4.9. In the lower pH range the surface hydroxyl of ZrO$_2$ in the MZF/P was protonated and positively charged and H$_2$PO$_4^-$ and HPO$_4^{2-}$ were the predominant aqueous species of phosphate. Then the electrostatic attraction generated between the negative phosphate anions and the positive protonated MZF/P surface, which facilitate the phosphate adsorption reaction. Increase of pH caused the deprotonation of surface sites and more negative surface potential of adsorbent, as well as the more negatively charged PO$_4^{3-}$ species, then the electrostatic
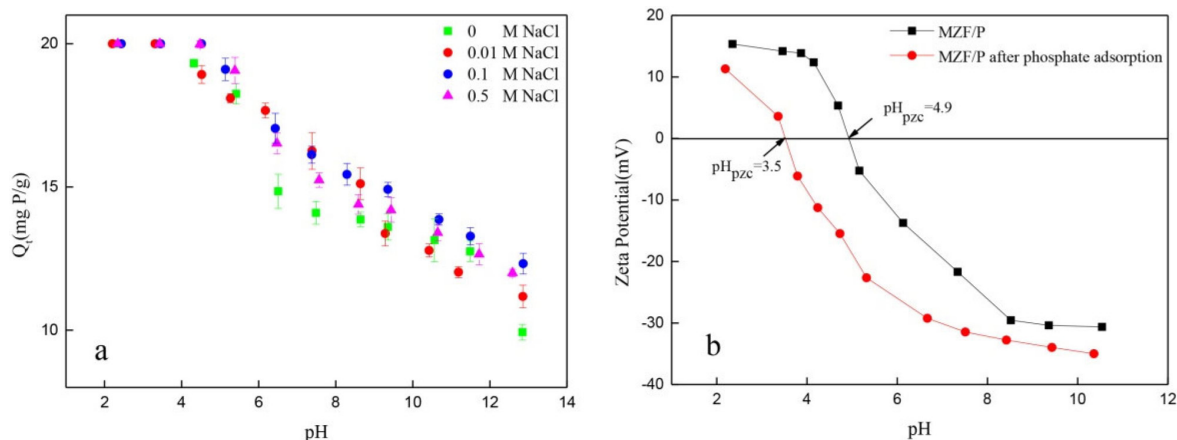
Figure 6. (**a**) Effects of pH and ionic strength; (**b**) Surface zeta potentials of MZF/P as a function of pH. (Initial concerntration: 50 mg L^{-1}; adsorbent dose: 2.5 g L^{-1}; contact time: 300 min; temperature: 25°C)

repulsive interaction between the phosphates anion and the negatively charged surface was invoked. Additionally, the lower adsorption at higher pH probably related to the competition between the phosphate ions and hydroxyl ions on the surface of the adsorbent.[25]

The surface zeta potentials of the MZF/P decreased after the phosphate adsorption and its isoelectric point shifted to 3.5. The isoelectric point is determined by protonation and deprotonation of surface hydroxyl groups. The formation of outer-sphere surface complexes could not lead to chemical reaction between the adsorbate and adsorbent surface and transform in the surface charge, which change the isoelectric point.[36] Thus, there is a specific adsorption rather than a purely electrostatic interaction existed between the phosphate and adsorbent and inner-sphere phosphate anionic charged surface complexes were formed due to an exchange reaction as following Eqs. (11) and (12).

$$Zr\text{-}OH + H_2PO_4^- = Zr(H_2PO_4) + OH^- \qquad (11)$$
$$2Zr\text{-}OH + HPO_4^{2-} = Zr_2(HPO_4) + 2OH^- \qquad (12)$$

As the ionic strength increased the phosphate adsorption almost unchanged at acidic conditions, but it was slightly enhanced at neutral to alkaline pH ranges. The similar situations for the phosphate adsorption on other adsorbents were also reported previously.[25,27] The ionic strength could strongly influence the adsorption of phosphate anions through outer-sphere association and the adsorption could be suppressed by competition with other anions such as Cl$^-$, since electrolytes also form outer-sphere complexes through electrostatic forces. Otherwise, phosphate adsorbed through inner-sphere association either show little sensitivity to ionic strength or respond to higher ionic strength with greater adsorption.[37] Thus, the adsorption of phosphate on MZF/P follows the inner-sphere complex mechanism.

There are always multiple coexisting anions in wastewater, which could give rise to potential competition for the adsorption sites with phosphate. The influences of the common anions on phosphate adsorption by MZF/P were inspected and the results were shown in Table 6. The presence of nitrate and sulfate made the adsorption capacities a little decrease and the citrate led to a great decline of adsorption. This may be a result of the competition between the phosphate and hydroxyl groups of citrate.[32] However, the coexistence of acetic increased the adsorption and caused a lower final pH, which was favorable to the phosphate adsorption.

Desorption of phosphate and reusability of MZF/P

The phosphate adsorption was basically inhibited at high pH,

Table 6. The effect coexisting anions on phosphate adsorption by MZF/P

Matrix	Final pH	Phosphate adsorption capacities (mg/g)
Phosphate only	3.38±0.16	19.622±0.248
+0.01 mol L^{-1} sodium nitrate	3.22±0.09	19.617±0.169
+0.01 mol L^{-1} sodium sulfate	3.39±0.13	19.601±0.314
+0.01 mol L^{-1} sodium citrate	4.37±0.21	13.210±0.227
+0.01 mol L^{-1} sodium acetic	2.34±0.11	19.928±0.035

so NaOH solution was used as an eluent to conduct phosphate desorption from the saturated adsorbent. The adsorbent experienced adsorption-desorption-regeneration cycle and the relationship between cycle number and adsorption capacity were displayed in Figure 7. The adsorption capacity of the original adsorbent MZF/P was signed 0 of the cycle number. Generally, the adsorption capacity should decrease gradually with an increase of the cycle number. The desorption rate of the first run was close to 93% and then stabilized in the range of 65-77%, indicating that phosphate adsorbed at partial adsorption points was not easily desorbed when desorption conditions were applied. More than 70% of the original phosphate capability on the adsorbent MZF/P could be retained through three cycles of desorption- reuse. The adsorption capability was 63% of the original adsorption after the fifth cycle. Though desorption conditions awaits further optimization, the reusability of MZF/P after desorption and regeneration is still feasible.
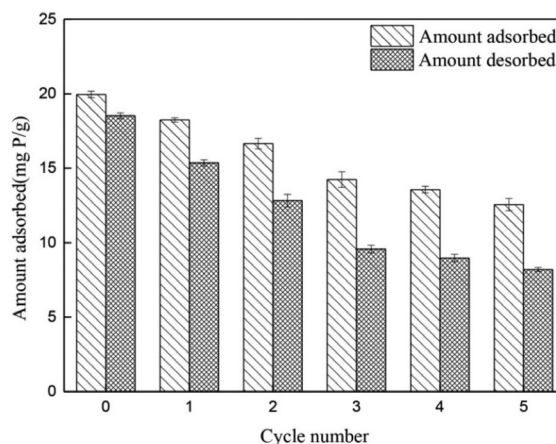

Figure 7. The results of desorption and regeneration experiments for MZF/P. (Initial concerntration: 50 mg/L; adsorbent dose: 2.5 g/L; contact time: 300 min; pH: 4.5; temperature: 25 °C)

FTIR, XRD, XPS analysis and adsorption mechanism

Figure 8 represented the FTIR spectra of the samples MF, MZF, MZF/P before and after phosphate adsorption. The broad band around 3418 cm^{-1} corresponded to the stretching vibration of OH and the peak near 1640 cm^{-1} was attributed to the bending vibration of water molecules. In the spectrum of MF the bands at 567 cm^{-1} and 432 cm^{-1} ascribed to the vibrations of Fe-O which were associated with Fe$_3$O$_4$.[23] The MZF illustrated peak at 1338 cm^{-1} corresponded to the deformation vibration of Zr-OH.[38] For the MZF/P the peak related to palygorskite appeared at 1024 cm^{-1} ascribed the Si-O bending vibration. There were some changes arising in the spectrum of MZF/P after phosphate adsorption. The peaks involving O-H bending vibration of 1640 and 1338 cm^{-1} were weakened significantly and almost disappeared, respectively. It was suggested that the surface hydroxyl groups were substituted by the phosphate and the adsorption mechanism of adsorbent MZF/P may be the ion exchange between the hydroxyl on the adsorbent surface and phosphate in the solution.[32]
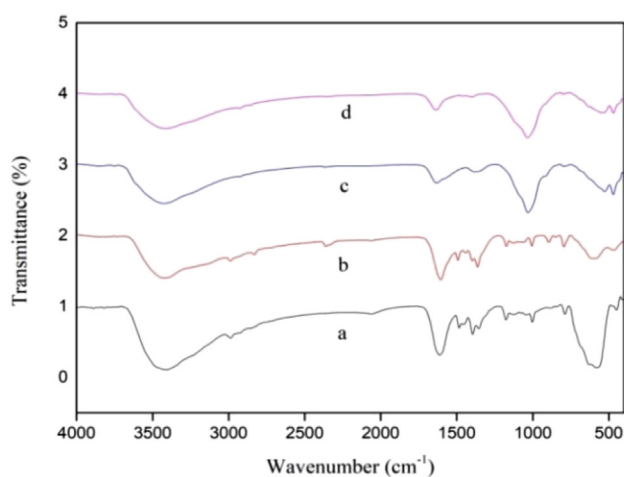
Figure 9. *XRD patterns of the samples MF(a), MZF(b), MZF/P(c) and MZF/P after adsorption(d)*

Figure 8. *FTIR spectra of the samples MF(a), MZF(b), MZF/P before(c) and after(d) phosphate adsorption*

XRD patterns of the samples MF, MZF, MZF/P and MZF/P after adsorption test were shown in Figure 9. It is shown that several strong peaks appeared at $2\theta = 30.1°$, $35.6°$, $43.2°$, $57.3°$, $62.9°$, which could be assigned to magnetite (JCPDS card #19-0629). There was not obvious difference on the XRD pattern between the MZF with the MF. It could be understood that the hydrous zirconia being amorphous
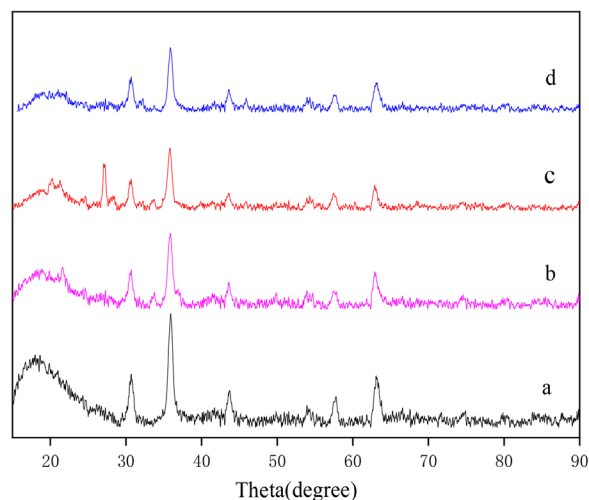
with a poor crystallinity should exhibit only one broad and weak peak at around 30.2° (zirconium oxide, PDF#37-1413), whose position just was overlapping with the magnetite. As to the XRD pattern of MZF/P, besides numbers of peak corresponding the magnetite located their position, the moderately strong diffraction peaks at 19.8° and 27.6° could be assigned to palygorskite. It suggested that the magnetic zirconium-iron oxides were well sediment on the surfaces of the palygorskite. No evident variation could be seen about MZF/P before and after phosphate adsorption. Thus, the adsorption of phosphate hardly changed the crystalline phase of magnetite and hydrous zirconia.

XPS studies of the MZF/P before and after phosphate adsorption at initial pH 4.5 were conducted to investigate the interactions between the MZF/P and phosphate. The interactions between the functional groups on the adsorbent and phosphate ions could be detected through the characteristic peak shift and intensity change in the XPS spectra. Figure 10(a) displayed the O 1s spectra of the adsorbent before and after phosphate adsorption. The peak at 531.98 eV in the O 1s spectrum for the original adsorbent can be assigned to hydroxyl group bonded to zirconium (Zr -OH).[39] After phosphate adsorption, the binding energy of O 1s shift to 531.81eV and the peak area ratio for the peak at 531.98 eV ascribed Zr-OH decreased from 27% to 23%, suggesting that hydroxyl groups on the MZF/P surface must be involved in the phosphate adsorption. This is consistent with the
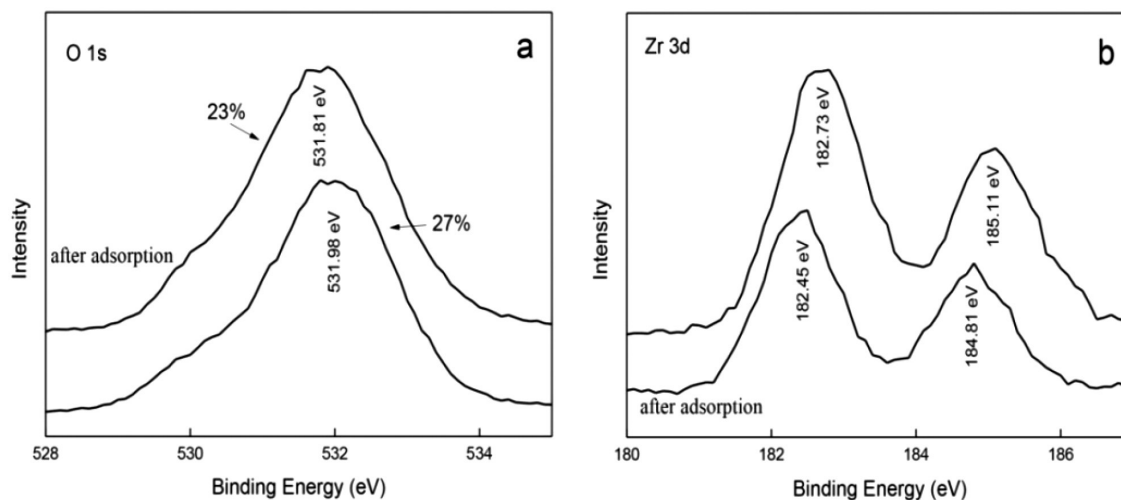
Figure 10. *XPS spectra of MZF/P before and after phosphate adsorption. (a) O 1s and (b) Zr 3d*

results of FT-IR analysis. The Zr 3d spectra of the adsorbent before and after phosphate adsorption were reported in Figure 10(b). It was observed the binding energies of 182.73 eV and 185.11 eV for Zr 3d, attributed to Zr 3d5/2 and Zr 3d3/2 respectively, indicating the presence of Zr(IV). The binding energies of the Zr 3d5/2 and Zr 3d3/2 moved to 182.45 eV and 184.81 eV, reduced by 0.28 eV and 0.3 eV, respectively. It indicated that there was a possible electron transfer in the valence band of Zr 3d and the formation of complexes, *i.e.* Zr species were also participate in the process of phosphate adsorption. This is in agreement with the adsorption of phosphate on the adsorbent via the ion-exchange mechanism noticed by other researches.[27,32]

CONCLUSIONS

The adsorbent MZF/P was produced by a simple co-precipitation technique using PLA as the carrier material for loading of magnetic zirconium-iron oxide nanoparticles, and its structures and performances of adsorption phosphate in aqueous solution were investigated. The specific surface area, pore volume and pore size of the MZF/P were slightly smaller than the MZF and the phosphate adsorption capacity of the MZF/P could basically reach about 90% of that of MZF at pH 4.5. The adsorption process agreed with the pseudo-second-order kinetic model and both Langmuir equation and D-R equation could well describe the adsorption isotherm. The monolayer saturation adsorption capacity was 38.2 mg/g at pH 4.5 and the mean energy of sorption was 16.12 kJ/mol. The adsorption showed little pH dependence at acidic conditions and decreased sharply with the pH increase above pH 5. The mechanism of adsorption phosphate on MZF/P followed the ion exchange between hydroxyl and phosphate accompanying a formation of inner-sphere complex. The adsorbent MZF/P could be desorbed and regenerated under alkaline conditions and the adsorption capability could maintain 63% of the original adsorption after 5 consecutive reuse cycles. The adsorbent MZF/P possessed essentially the same phosphate adsorption efficiency and lower production costs comparing with MZF and it is expected to be considered for cost-feasible treatment of phosphate.

ACKNOWLEDGMENTS

REFERENCES

1. Xu, Q.; Liu, X.; Wang, D.; Wu, Y.; Wang, Q.; Liu, Y.; Li, X.; An, H.; Zhao, J.; Chen, F.; Zhong, Y.; Yang, Q.; Zeng, G.; *Chemosphere* **2018**, *213*, 276. [Crossref]

2. Lalley, J.; Han, C.; Li, X.; Dionysiou, D. D.; Nadagouda, M. N.; *Chem. Eng. J.* **2016**, *284*, 1386. [Crossref]

3. You, K.; Yang, W.; Song, P.; Fan, L.; Xu, S.; Li, B.; Feng, L.; *Colloids Surf., A* **2022**, *633*, 127897. [Crossref]

4. Aswin Kumar, I.; Jeyaseelan, A.; Viswanathan, N.; Naushad, M.; Valente, A. J. M. J.; *Solid State Chem.* **2021**, *302*, 122446. [Crossref]

5. Ni, F.; He, J.; Wang, Y.; Luan, Z.; *J. Water Process Eng.* **2015**, *6*, 158. [Crossref]

6. Tran, T. T.; Tran, N. N. T.; Sugiyama, S.; Liu, J. C.; *J. Mater. Cycles Waste Manage.* **2021**, *23*, 177. [Crossref]

7. Ajmal, Z.; Muhmood, A.; Usman, M.; Kizito, S.; Lu, J.; Dong, R.; Wu, S.; *J. Colloid Interface Sci.* **2018**, *528*, 145. [Crossref]

8. Mitrogiannis, D.; Psychoyou, M.; Baziotis, I.; Inglezakis, V. J.; Koukouzas, N.; Tsoukalas, N.; Palles, D.; Kamitsos, E.; Oikonomou, G.; Markou, G.; *Chem. Eng. J.* **2017**, *320*, 510. [Crossref]

9. Luo, W.; Huang, Q.; Zhang, X.; Antwi, P.; Mu, Y.; Zhang, M.; Xing, J.; Chen, H.; Ren, S. J.; *Water Process. Eng.* **2020**, *33*, 101036. [Crossref]

10. Xia, M.; Gao, R.; Wang, Y.; Wang, S.; Yun, Y.; Dou, J.; *Environ. Technol. (UK)* **2021**, *42*, 1652. [Crossref]

11. Zamparas, M.; Kyriakopoulos, G. L.; Drosos, M.; Kapsalis, V. C.; *Molecules* **2021**, *26*, 6684. [Crossref]

12. Xi, H.; Jiang, H.; Zhao, D.; Zhang, A. H.; Fan, B.; Yang, Y.; Zhang, J.; *J. Clean. Prod.* **2021**, *313*, 127773. [Crossref]

13. Wu, Y.; Li, X.; Yang, Q.; Wang, D.; Xu, Q.; Yao, F.; Chen, F.; Tao, Z.; Huang, X.; *J. Environ. Manage.* **2019**, *231*, 370. [Crossref]

14. Li, G.; Yang, M.; Ding, X.; Tan, W.; Li, G.; Fang, S.; Wang, H.; *Desalin. Water Treat.* **2021**, *237*, 64. [Crossref]

15. Goscianska, J.; Ptaszkowska-Koniarz, M.; Frankowski, M.; Franus, M.; Panek, R.; Franus, W.; *J. Colloid Interface Sci.* **2018**, *513*, 72. [Crossref]

16. Pergher, S. B. C.; Oliveira, L. C. A.; *Quim. Nova* **2005**, *28*, 751. [Crossref]

17. Dali Youcef, L.; Belaroui, L. S.; López-Galindo, A.; *Appl. Clay Sci.* **2019**, *179*, 105145. [Crossref]

18. Dong, L.; Lin, L.; Li, Q.; Huang, Z.; Tang, X.; Wu, M.; Li, C.; Cao, X.; Scholz, M.; *J. Environ. Manage.* **2018**, *213*, 151. [Crossref]

19. Johir, M. A. H.; Pradhan, M.; Loganathan, P.; Kandasamy, J.; Vigneswaran, S.; *J. Environ. Manage.* **2016**, *167*, 167. [Crossref]

20. Vereshchagin, A. O.; Mashkovtsev, M. A.; Pribytov, M. D. *AIP Conf. Proc.* **2020**, *2313*, 050037. [Crossref]

21. Huo, J.; Min, X.; Wang, Y.; *Environ. Res.* **2021**, *194*, 110685. [Crossref]

22. Chen, Z.; Luo, H.; Rong, H.; *Int. J. Biol. Macromol.* **2020**, *164*, 1183. [Crossref]

23. Liu, Y.; Liu, P.; Su, Z.; Li, F.; Wen, F.; *Appl. Surf. Sci.* **2008**, *255*, 2020. [Crossref]

24. Eaton, A. D.; Franson, M. A. H.; *Standard Methods for the Examination of Water & Wastewater*, American Public Health Association, 2005.

25. Zhang, C.; Li, Y.; Wang, F.; Yu, Z.; Wei, J.; Yang, Z.; Ma, C.; Li, Z.; Xu, Z. Y.; Zeng, G.; *Appl. Surf. Sci.* **2017**, *396*, 1783. [Crossref]

26. Wang, Y.; Liu, D.; Lu, J.; Huang, J.; *Colloids Surf., A* **2015**, *481*, 133. [Crossref]

27. Wang, Z.; Xing, M.; Fang, W.; Wu, D.; *Appl. Surf. Sci.* **2016**, *366*, 67. [Crossref]

28. Wang, W.; Zhang, H.; Zhang, L.; Wan, H.; Zheng, S.; Xu, Z.; *Colloids Surf., A* **2015**, *469*, 100. [Crossref]

29. Xiong, W.; Tong, J.; Yang, Z.; Zeng, G.; Zhou, Y.; Wang, D.; *J. Colloid Interface Sci.* **2017**, *493*, 17. [Crossref]

30. Sun, Q.; Yang, L.; *Water Res.* **2003**, *37*, 1535. [Crossref]

31. Hsieh, C. T.; Teng, H.; *J. Chem. Technol. Biotechnol.* **2000**, *75*, 1066. [Crossref]

32. Long, F.; Gong, J.; Zeng, G.; Chen, L.; Wang, X.; Deng, J.; Niu, Q.; Zhang, H.; Zhang, X.; *Chem. Eng. J.* **2011**, *171*, 448. [Crossref]

33. Kim, B. T.; Lee, H. K.; Moon, H.; Lee, K. J.; *Sep. Sci. Technol.* **1995**, *30*, 3165. [Crossref]

34. Benhammou, A.; Yaacoubi, A.; Nibou, L.; Tanouti, B.; *J. Colloid Interf. Sci.* **2005**, *282*, 320. [Crossref]

35. Liu, H.; Sun, X.; Yin, C.; Hu, C.; *J. Hazard. Mater.* **2008**, *151*, 616. [Crossref]

36. Su, Y.; Cui H.; Li, Q.; Gao, S.; Shang, J. K.; *Water Res.* **2013**, *47*, 5018. [Crossref]

37. Ren, Z.; Shao, L.; Zhang, G.; *Water Air Soil Pollut.* **2012**, *223*, 4221. [Crossref]

38. Cui, H.; Li, Q.; Gao, S.; Shang, J. K.; *J. Ind. Eng. Chem.* **2012**, *18*, 1418. [Crossref]

39. Zhang, G.; He, Z.; Xu, W.; *Chem. Eng. J.* **2012**, *183*, 315. [Crossref]